LHCB-MUON 2001-120
Version 2.0 4th December 2001

Test of a double gap MWPC for the region 3 of the LHCb muon system

M. Anelli, C. Bloise, P. Campana, G. Felici, C. Forti, M. Palutan, A. Saputi, A. Sciubba
Laboratori Nazionali dell'INFN, Frascati, Italy

G. Pirozzi
Università della Basilicata, Potenza and Sezione INFN Roma I, Italy

Abstract

We present the first results obtained with a double gap prototype of MPWC with cathode readout for the region 3 of the LHCb muon system. Preliminary studies on the efficiencies, on the crosstalk, on time resolution and uniformity for both cathode and anode readout are reported. The performances appear to match the requests of the LHCb muon system. In the appendix we report the measurement for a second double gap tested in a further testbeam session.

Contents

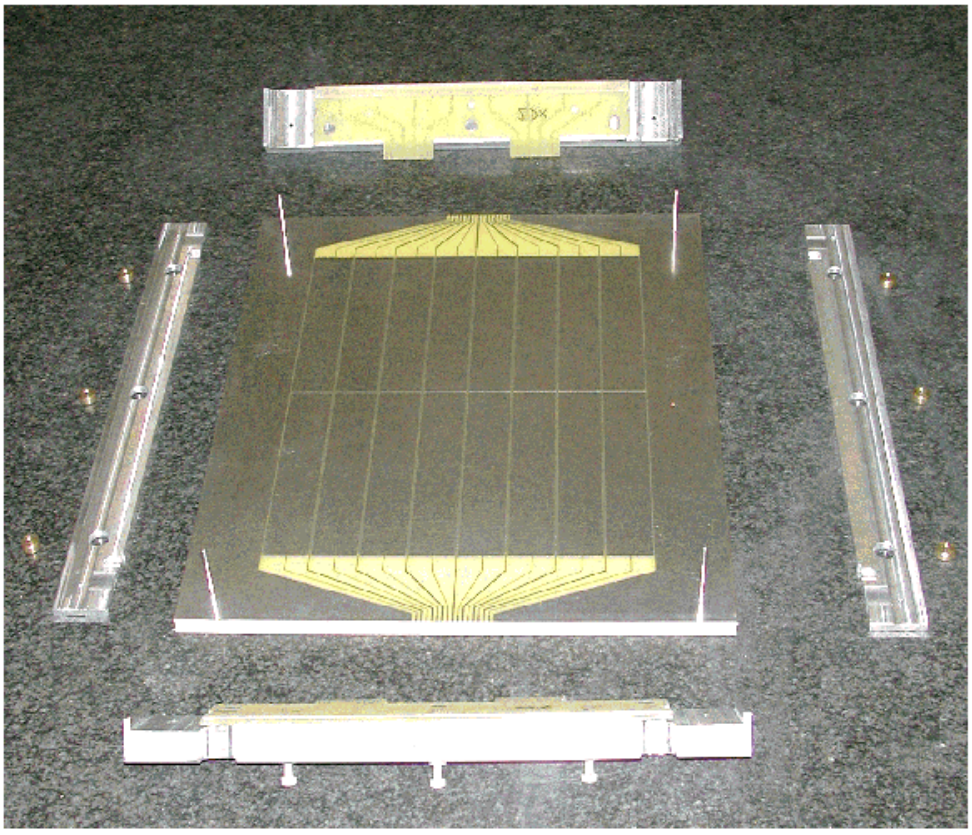

Figure 1: A picture of the cathode plane before the assembly.

1 Introduction

In this note we report the results of a test of a MWPC, assembled in Frascati Laboratories of INFN, designed for the muon system of the LHCb experiment. This prototype was built with the aim to study the validity of the mechanical design and of the construction procedures. In Section 2 we provide a description of the detector, including geometry, signal readout and electronics. Then, in Section3 we report the testbeam results, with particular emphasis on current and efficiency studies, thresholds, spatial uniformity, time window amplitude and position, crosstalk effects. The detector time resolution is also estimated. In last Section, we draw the conclusions of the test. In the Appendix we report the results obtained with another double gap in September 2001 testbeam, and we compare them with the previous test results.

2 Prototype description

2.1 Detector layout

A schematic view of the prototype is shown in Fig. 2, a top view of the wire plane and of the underlying cathode plane. The sensitive area of the chamber is $\sim 200 \times 251$ mm^2, representing 1/6 of one final WPC for region M2R3. The prototype is composed of two gaps, each with an anode wire plane at the center of the gap, a plane of cathode pads and a ground plane.

In Fig. 3 we show the chamber cross-sections at two opposite sides: on the right the cathode pad readouts, on the left the wire pad readouts.

In Fig. 4 we show a blow up of the wire fixation bar.

The main chamber parameters are reported in Table 1.

Outer chamber dimensions	$279 \times 341 \times 45$ mm^3	Sensitive area	200×251 mm^2
Panels thickness	10 mm	Foam thickness	8 mm
N. of gaps	2	Gap size	5 mm
N. of wire pads	2×8	N. of cathode pads	2×16
N. of anode readouts	8	N. of cathode readouts	16 (8 in this test)
N. of wires	2×134	Wire pitch	1.5 mm
Wire diameter	30 μm	Wire tension	50 g
Wire pad size	25×250 mm^2	Cathode pad size	25×125 mm^2

Table 1: MWPC prototype parameters. Numbers refer to the full chamber (bigap). In this test we read out only half of the cathode pads of each gap. The two gaps are in OR both for cathode and for wire pad readouts.

2.2 Chamber components

The main components of our prototype are the following:

- Panels: they are obtained injecting a rigid polyurethanic foam (ESADUR 120) between two FR4 printed circuit boards. Three panels were used: the two bottom panels of each gap were etched on the top side to provide the cathode pad structure. A third panel (not etched) act as a cover for the top gap.
- Frames: two FR4 non machined wire fixation bars, 2.4 mm thick, on left and right sides of the chamber (as shown in Fig. 2). Over each of them, there is a gap bar to close the gas gap. On top and bottom sides, there are non machined Al bars, 4.9 mm thick, with

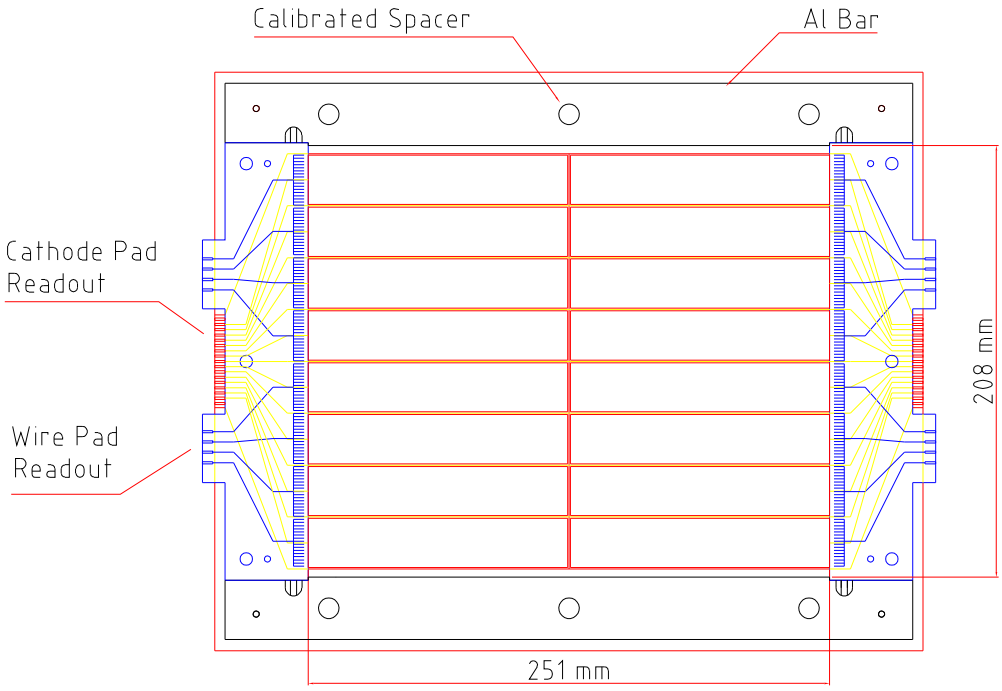

Figure 2: Top view of the wire plane laying over the cathode plane. This is the point of view of the impinging particles, with chamber perpendicular to the beam and pads parallel to horizontal X axis.

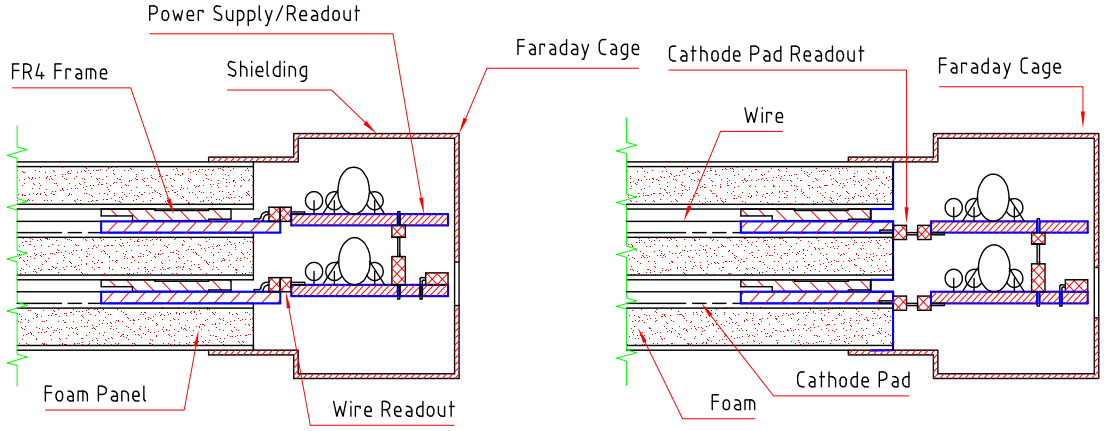

Figure 3: Detector cross sections showing in detail the cathode pad readouts (right) and the wire pad readouts (left).

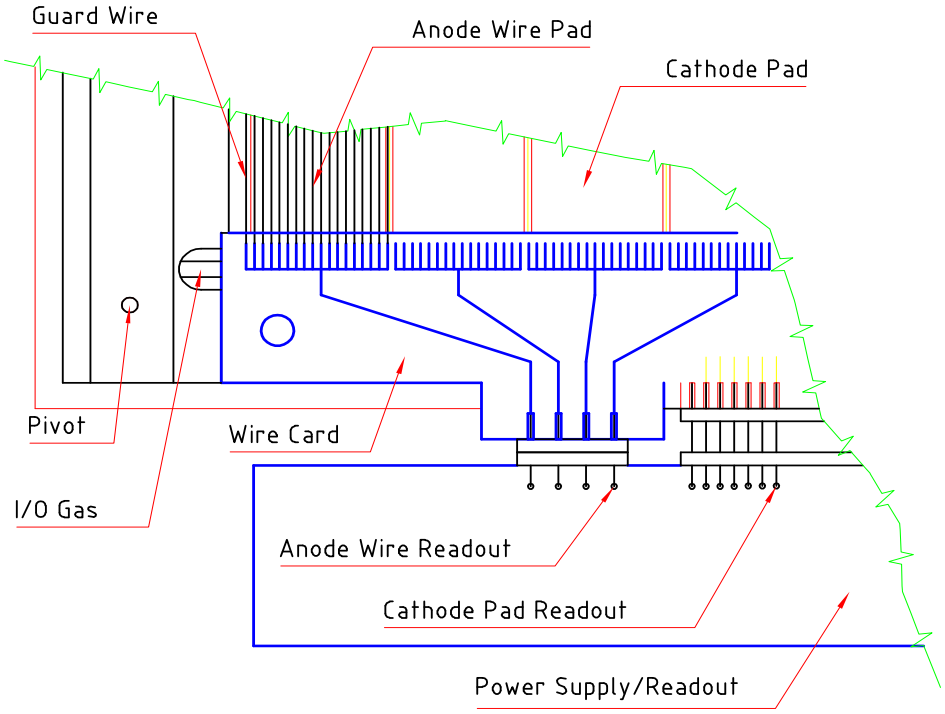

Figure 4: Detailed top view.

the gas inlets. The gap dimension is kept precise to $\pm 20 \mu$m using calibrated spacers (for more details on the construction technique, see pp. 43-47 of [1]).

– Wires: the gold-plated tungsten wires were hand-wired at 50 g tension, manually soldered, and glued.

2.3 Signal readout

To get a more exhaustive information, although this prototype is designed for the R3 region (where only cathode pads will be read out) the anode wire pads signals were read as well.

Both the cathode and anode readout and the HV distribution system are done on removable cards plugged as shown in Fig. 3.

2.3.1 Anode wire readout

As usual, the readout design takes into account the reduced space between chambers. Particular care has been taken in separating as much as possible HV lines and capacitors from ground.

The signals were OR-ed in the HV board before they pass in the preamplifier. The innovative solution of using external HV board hosting resistors and capacitors, makes the readout design simple and robust even in the case of very high density connectors. Furthermore, an easy access at the HV distribution is left without the need to dismount the chambers or to open them.

2.3.2 Cathode pad readout

Referring to Fig. 2, while the wire extend from left to right and have about the same length as the chamber (~ 25 cm), the cathode pads are interrupted in the center by a gap of ~ 1.3 mm.

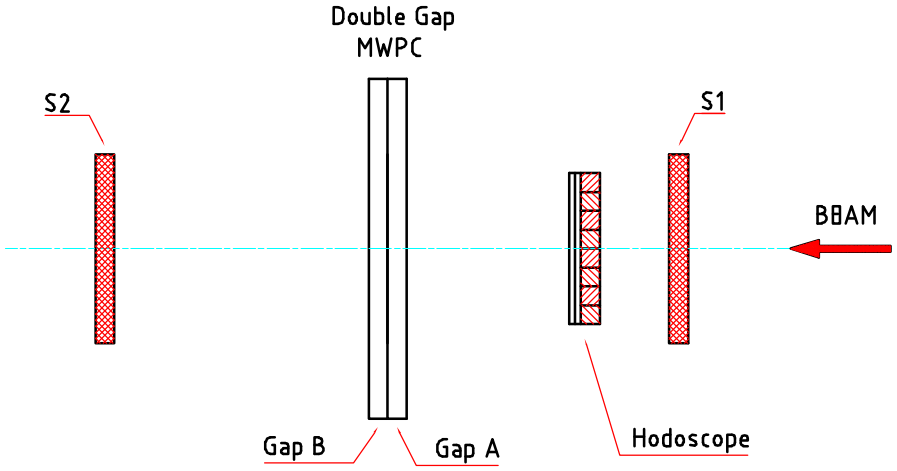

Figure 5: Layout of the experimental setup, including the two scintillators used for the trigger and the hodoscope used for geometrical selection of the beam (see Section 3.1.1).

In the middle of this gap there is a 0.5 mm ground strip. So, the number of cathode pads (16) is twice the number of wire pads (8) for each gap.

Due to the readout of 8 wire pads on one side, in the present test only 8 cathode pads on the opposite side were readout, putting in 'or' the signals of the two gaps.

2.4 Front End Electronics

The Front End Electronics used for this test is the most updated version of the usual ([2]) ASDQ++ chip board and spark protection board.

A dedicated NIM controller powered the boards and set the ASDQ thresholds.

As shown in Fig. 3, a copper Faraday cage was built surrounding the whole detector, in such a way to minimize the noise pick-up.

3 Testbeam results

3.1 Description of experimental setup

The experimental setup is shown in Fig. 5. The trigger was based on the coincidence of scintillators S_1 and S_2. The informations from vertical and horizontal channels of a hodoscope were used in the data analysis to identify the beam position respect to the chamber (Section 3.1.1).

3.1.1 Geometrical selection with hodoscope

The hodoscope consists of two planes, each with 8 scintillator strips (8×1 cm^2); one plane has horizontal strips, the other has vertical strips.

In Fig. 6 we show the density of particles on the hodoscope area. The crossing of one vertical strip ($Hodo_V$) with one horizontal strip ($Hodo_H$) defines an area of 1×1 cm^2. On the plot, the area of each box is proportional to the number of particles going through the corresponding square region. The beam spread is: σ_x=1.3 cm in horizontal coordinate; σ_y=0.8 cm in vertical coordinate.

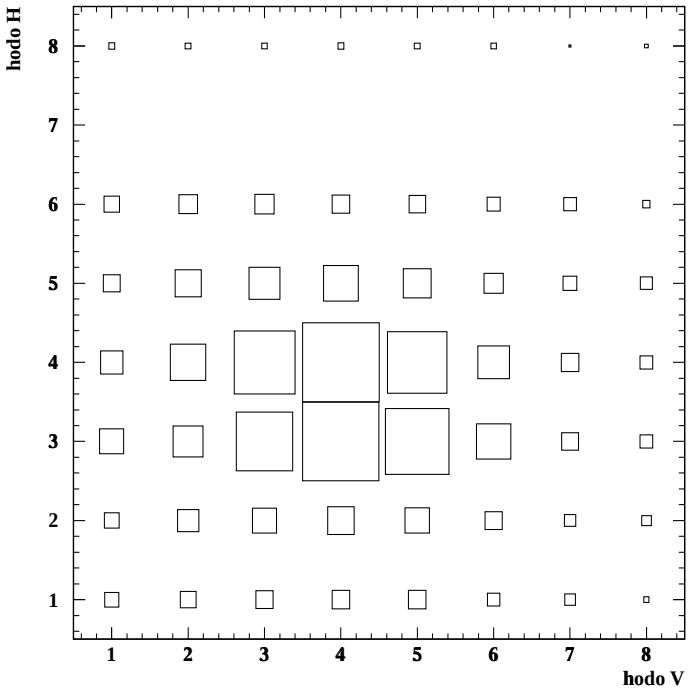

Figure 6: Hodoscope illumination. Each strip is large 1 cm. Horizontal channel # 7 was broken.

A large fraction of the beam can be selected requiring:

$$(Hodo_V = 3.OR.4.OR.5).AND.(Hodo_H = 3.OR.4)$$

For a study of the detector spatial uniformity (Section 3.7), or in the measurement of the efficiency near the chamber horizontal and vertical edges, a selection of a single hodoscope 'slice' is applied (respectively a vertical and a horizontal one) to minimize the size of the "effective" beam seen by the chamber.

The same solution has been adopted for time response and crosstalk studies, were we want to select a single pad crossed by the beam (see Section 3.6).

3.2 Current in the chamber

The two gaps showed since the beginning very low currents. In Fig.7 we show the maximum total current per gap, during the beam burst, as function of the high voltage setting. The currents are shown in the three consecutive days of the test session. The effect of conditioning is clear: for instance the current at 3300 V decreases from $\sim$500 nA to $\sim$100 nA. After conditioning, the current is < 100 nA up to 3300 V, and is $\sim \ 40 \div 45$ nA at the standard operation HV of 3150 Volts.

The maximum current per gap with beam OFF is also shown in Fig.7 (empty dots): for HV$\leq$3300 V the current value stays always below 8 nA, with very little time dedicated to conditioning.

3.3 Detector efficiency

To determine the efficiency of these pads we can use different methods, compared in figures 8 and 9 and described below:

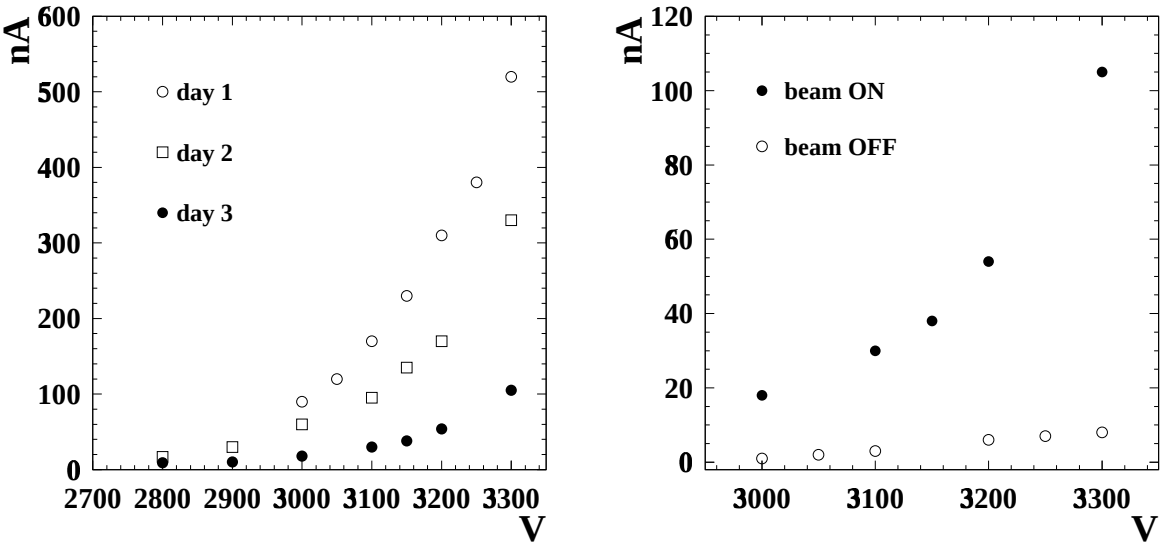

Figure 7: Maximum current in one gap as function of the high voltage applied. LEFT: with beam ON RIGHT: comparison of beam ON (after conditioning) with beam OFF. Thresholds are: Cathodes=250 mV Wires=350 mV.

- Method 1: we use the time spectrum of the first hit (fastest hit) among the 8 hits. We accept events in a time window of 20 ns, centered in a position (offset) that maximises the efficiency. The dependences of the efficiency on window length and offset are discussed in Section 3.5.
- Method 2: we take the logical OR of the 8 hits in a large time window (100 ns). Then, this "global" efficiency is multiplied by the ratio between the number of events in 20 ns and the total number of events in 100 ns for a single pad spectrum.
- Method 3: we take the logical OR of the 8 hits, each of them in its proper time window. The window length is the same for all spectra (20 ns) but the offset may differ from one spectrum to another.

The difference between the three methods is of the order of 1%.

For all results reported in this Section, the chamber efficiency is obtained with the first method (fastest hit spectrum).

For example, in Fig. 10 we compare the efficiency obtained with each single gap, with the full detector (bi-gap) efficiency. The results obtained with the two gaps are in very good agreement: in particular if we choose a low high voltage value (HV = 2900 V), where the efficiency is more sensitive to detector disuniformities, the difference between the two gaps is $\sim 1.5\%$ for cathode pads and $\sim 3\%$ for wire pads.

To appreciate better the shape of the efficiency plateaux, in Fig. 11 we show the efficiency curves in a smaller range of high voltage. Note that the wire pad curve for the bi-gap was obtained at threshold 270 mV, because at higher threshold (350 mV) the curve saturates at 98.5%.

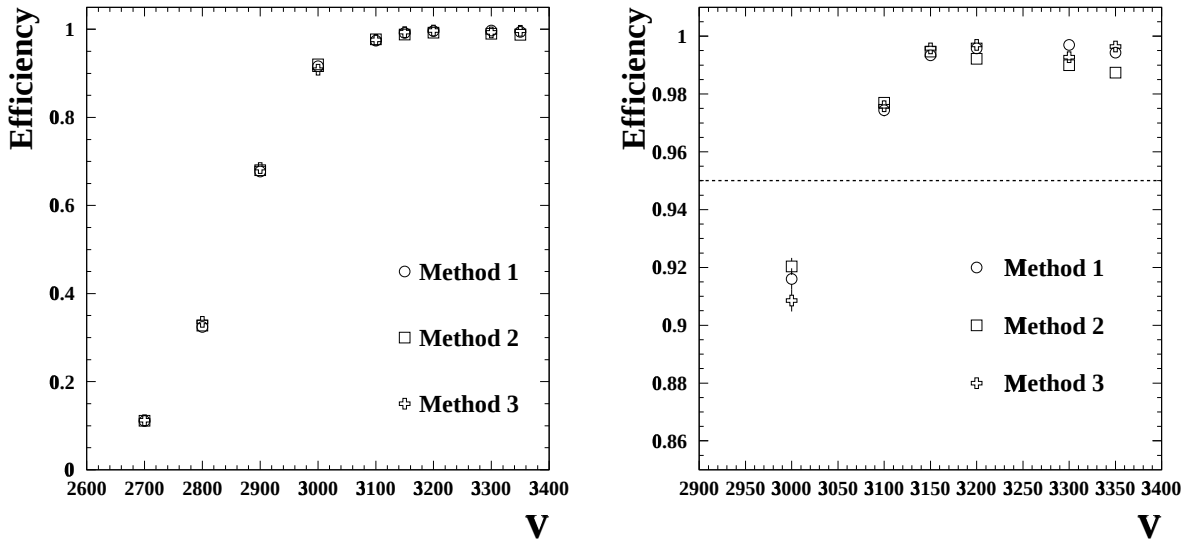

Figure 8: Cathode Pad efficiency, as function of the high voltage setting, determined with the three methods described in the text. The efficiency of one specific pad is also shown. Threshold is 300 mV. In (right) we show a zoom of (left).

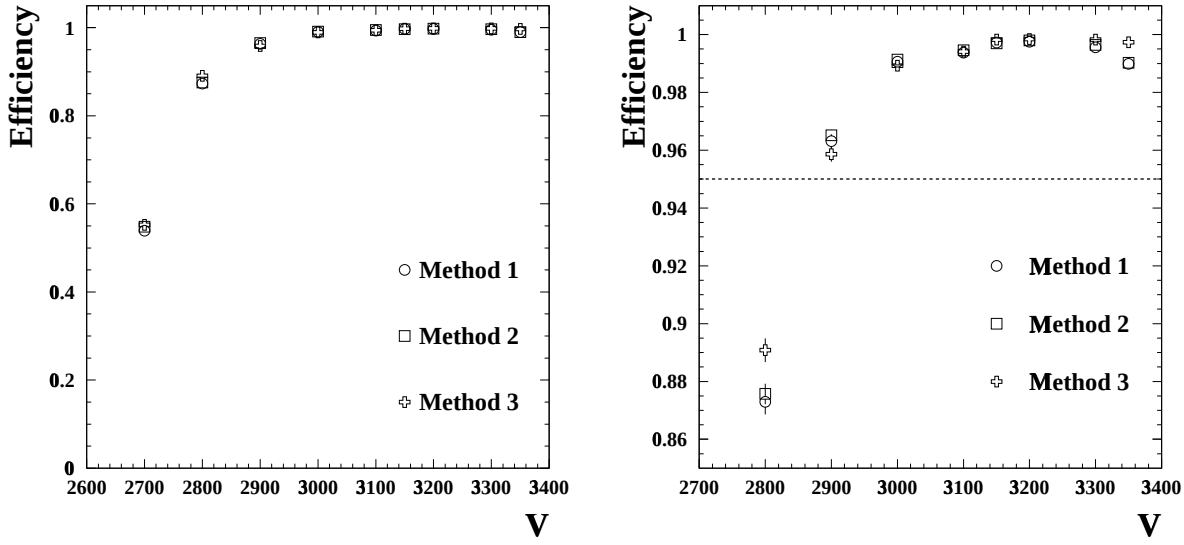

Figure 9: Wire Pad efficiency, as function of the high voltage setting, determined with the three methods described in the text. The efficiency of one specific pad is also shown. Threshold is 270 mV. In (right) we show a zoom of (left).

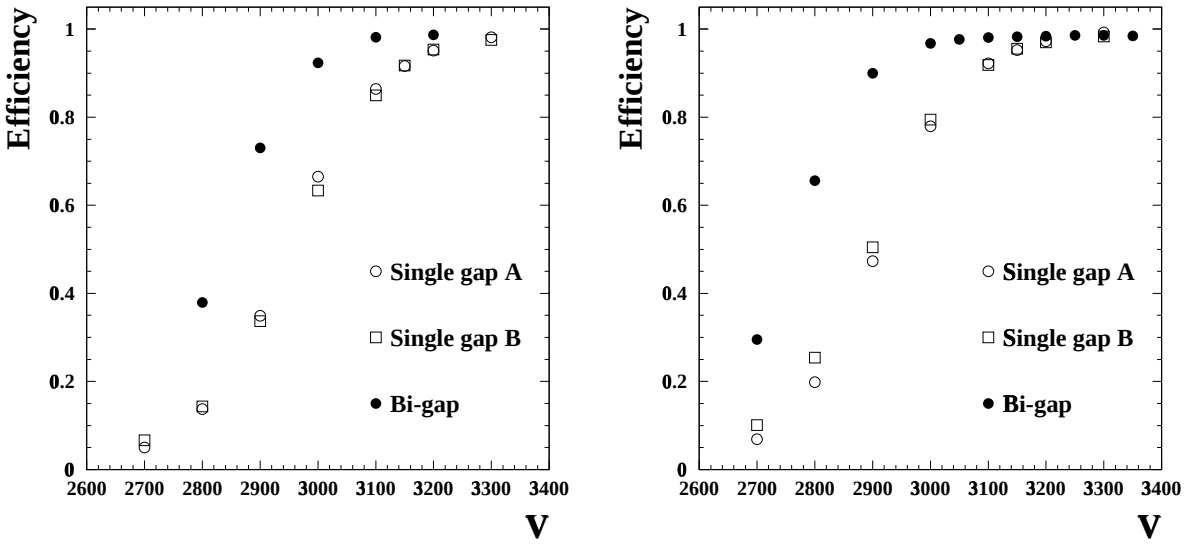

Figure 10: Efficiency for (left) cathode pads and (right) wire pads, as function of the high voltage setting. Measurements for each single gap configuration (only A with B off, only B with A off) are compared to the full detector (bi-gap). Thresholds are: Cathodes=300 mV Wires=270 mV.

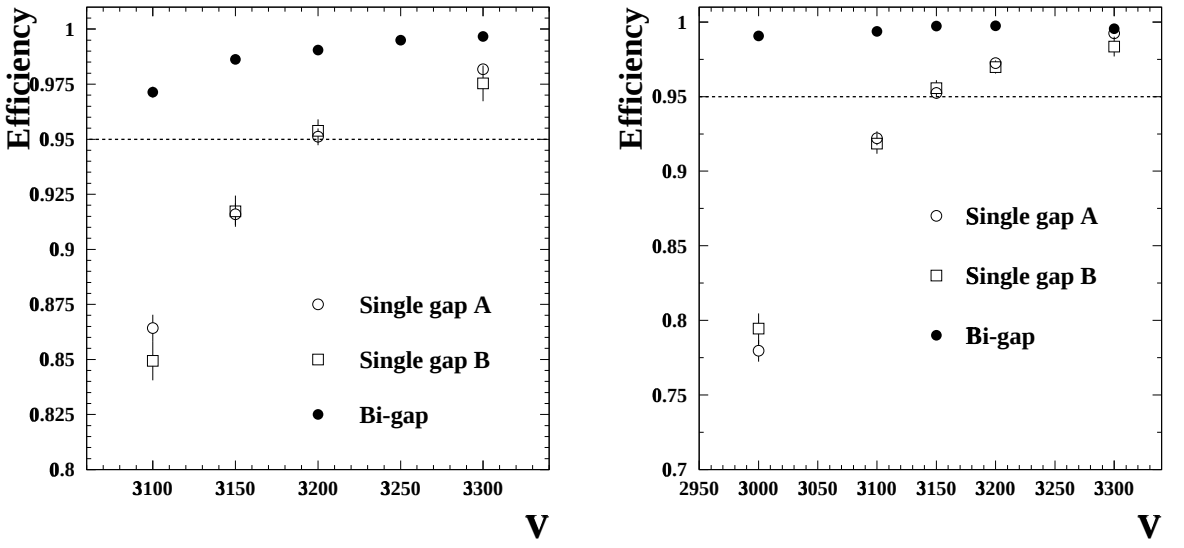

Figure 11: Efficiency for (left) cathode pads and (right) wire pads, as function of the high voltage setting. Measurements for each single gap configuration (only A with B off, only B with A off) are compared to the full detector (bi-gap). Thresholds are: (left) 250 mV for single gap, 300 mV for bi-gap; (right) 350 mV for single gap, 270 mV for bi-gap;

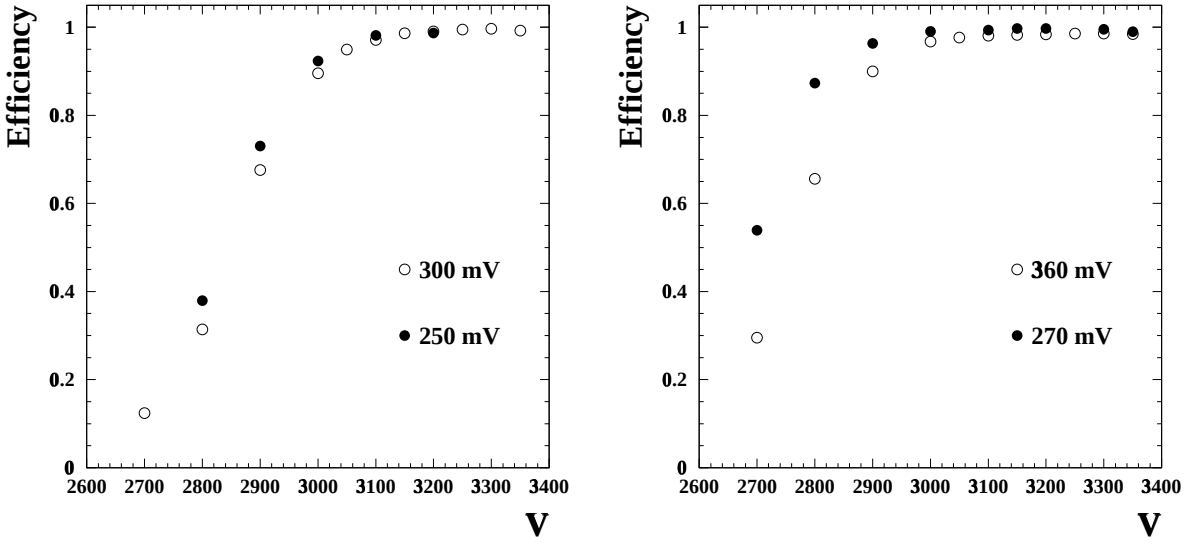

Figure 12: Efficiency for (left) cathode pads and (right) wire pads, as function of the high voltage, for different threshold settings. Time window length is 20 ns. Hodoscope pads selected are: vertical=3,4,5; horizontal=3,4.

3.4 Effects of varying the thresholds

In Fig. 12 the cathode and anode pad efficiencies are shown, as function of the high voltage applied, for two different threshold settings. As expected, the sensitivity on threshold decreases when high voltage increases. In a 20 ns time window, operating at 3150 V, we get $\epsilon = 99\%$ for cathode and $\epsilon = 99.7\%$ for anodes.

3.5 Time spectra and resolution

All results reported in this Section (time spectra, time resolution, etc...) refer to a single cathode pad (the # 7) and a single wire pad (the # 2), the best centered respect to the beam axis. For this reason we selected events with the hodoscope horizontal slice ($Hodo_H = 3$) fired.

In Fig.13 we show the time spectra for two different high voltage settings, for cathode and wire pads. We notice that the spectra are not precisely gaussian.

For this reason, we have not measured the time resolution with the usual gaussian fit. In Fig.14 we report the Root Mean Square (RMS) of the time spectra, as function of the high voltage applied. For high voltage at 3150 V, we find $\sigma(t) = 3.5$ ns for cathode pads and $\sigma(t) = 3.1$ ns for wire pads. A gaussian fit limited to the peak of the curve, gives as a result a σ that is about 1 ns smaller than the RMS of the whole distribution.

The position of the peak as function of the HV is also shown. The shift is small: $\delta_{peak} \sim$ 2 ns/100 V.

We measured the effect of varying the time window in which the signals are accepted. In Fig.15 we show the efficiency for cathode pads as function of the time window length and offset (with a fixed 20 ns time window). The same measurement for wire pads is shown in Fig.16. A summary of measurements is reported in Table 2.

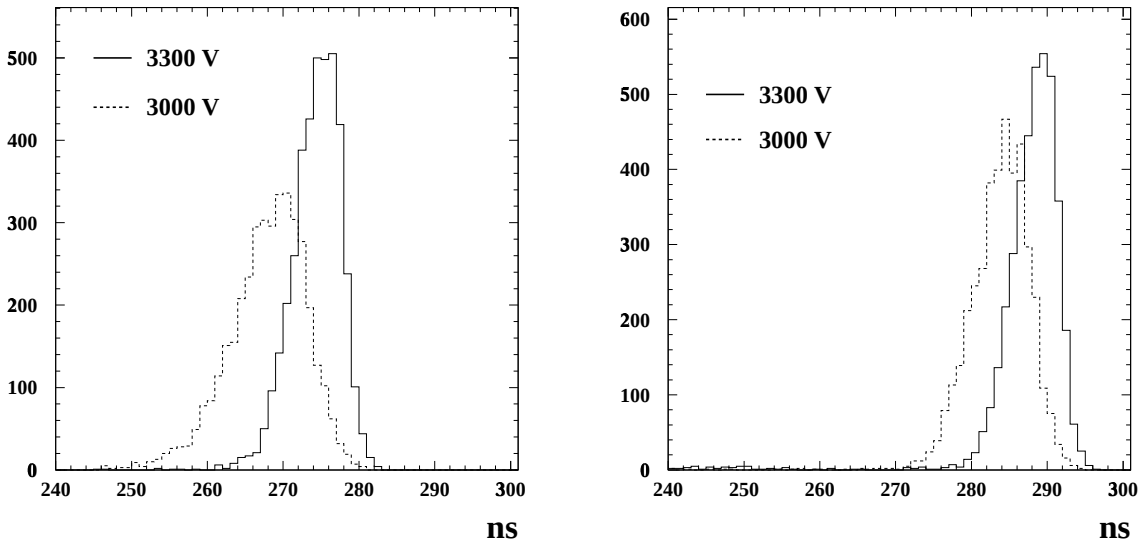

Figure 13: Time distribution for (left) single cathode pad and (right) single wire pad, at two HV settings. Thresholds are: Cathodes=300 mV Wires=270 mV.

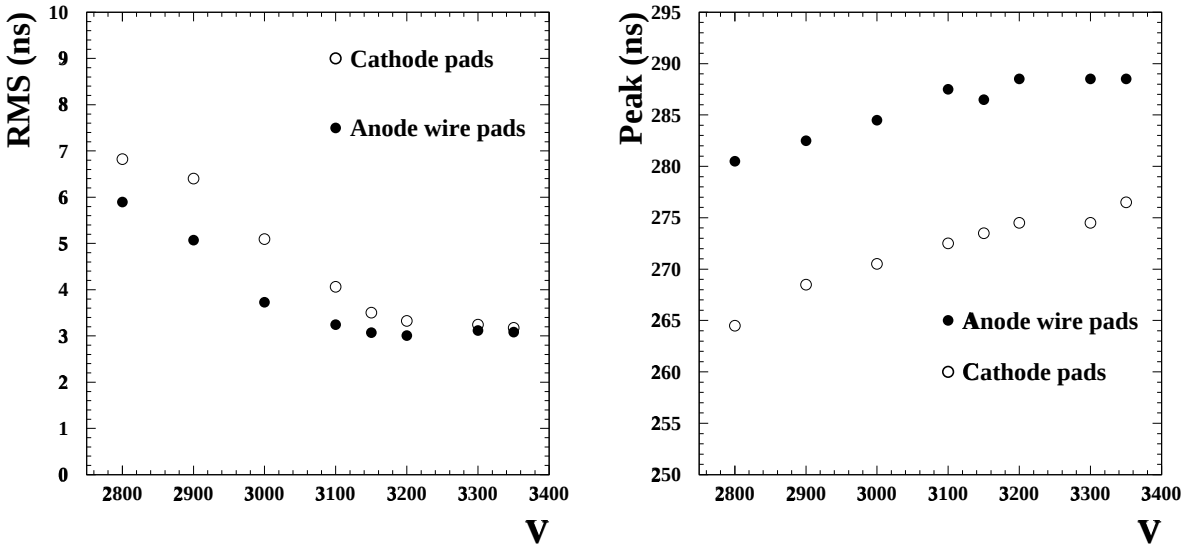

Figure 14: Time distribution RMS (left) and peak position (right), for single cathode pad and single wire pad, as function of the high voltage setting. Thresholds are: Cathodes=300 mV Wires=270 mV.

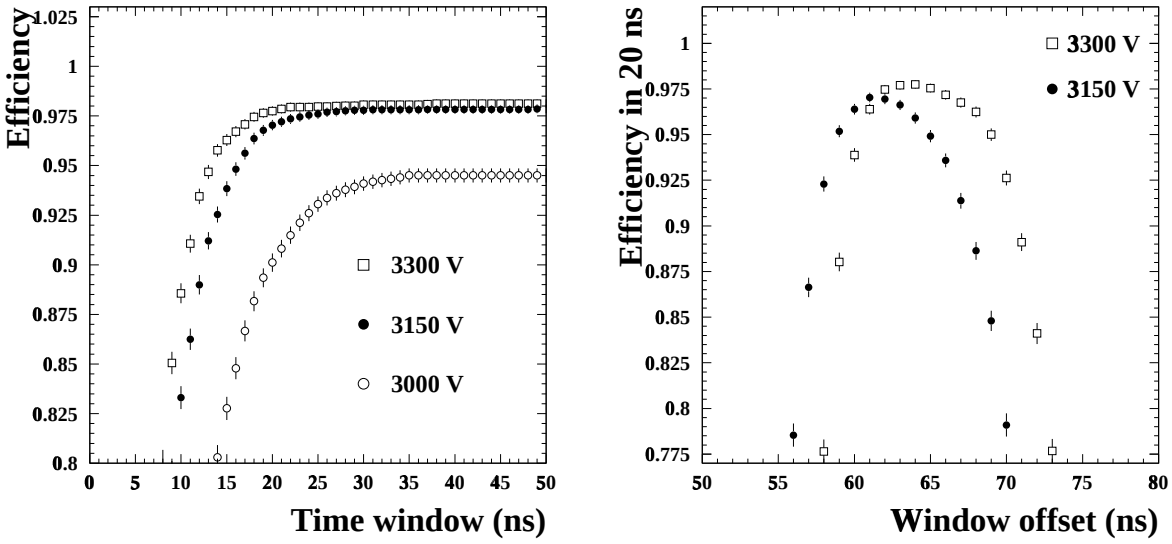

Figure 15: Efficiency for single cathode pad as function of the time window acceptance (left) and offset (right) for several high voltage settings. For each window length (left), the position of the window (window offset) is the one which maximises the efficiency. The offset dependence (right) is calculated for a fixed window length (20 ns). Thresholds are: Cathodes=300 mV Wires=270 mV.

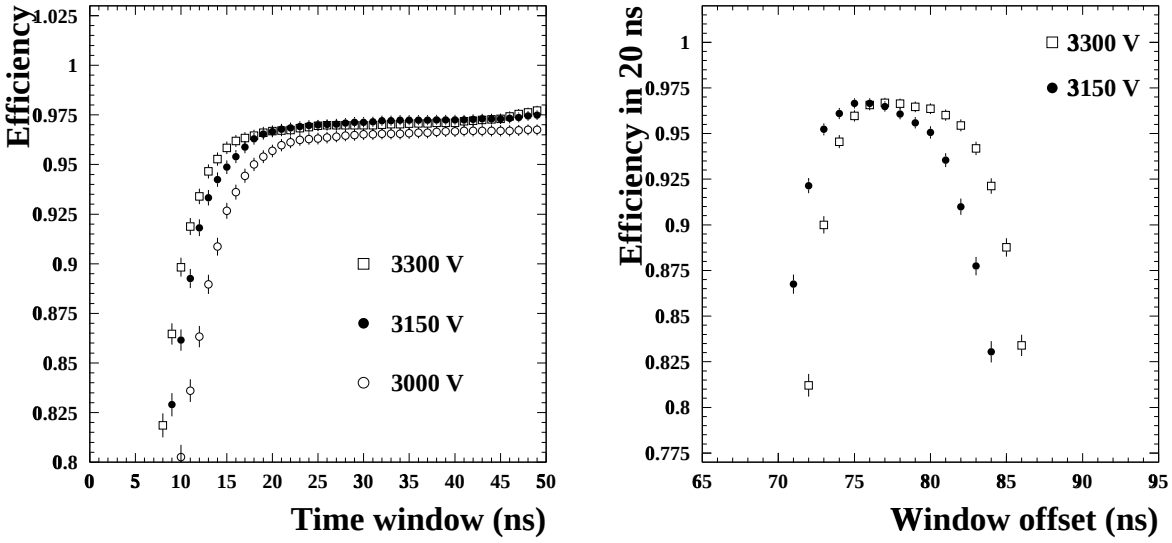

Figure 16: Efficiency for single wire pad as function of the time window acceptance (left) and offset (right) for several high voltage settings. For each window length (left), the position of the window (window offset) is the one which maximises the efficiency. The offset dependence (right) is calculated for a fixed window length (20 ns). Thresholds are: Cathodes=300 mV Wires=270 mV.

Cathode Pads				Wire Pads			
High Voltage (V)	3000	3150	3300	High Voltage (V)	3000	3150	3300
$\epsilon_{20}/\epsilon_{50}$	.953	.992	.996	$\epsilon_{20}/\epsilon_{50}$	.990	.994	.996
$\Delta t(\epsilon > 95\%)$	-	6	8.5	$\Delta t(\epsilon > 95\%)$	-	7	8.5

Table 2: $\epsilon_{20}/\epsilon_{50}$ is the ratio between the efficiency for a time window of 20 ns and the efficiency for a time window of 50 ns. $\Delta t(\epsilon > 95\%)$ is the width (in ns) of the offset range for which the efficiency is larger than 95%. Thresholds are 270 mV (Wires) and 300 mV (Cathodes).

3.6 Hit multiplicity and crosstalk

For a proper study of the crosstalk, we must guarantee that the beam crosses only one pad of the detector. Since both anode and cathode pads are horizontal slices, we select events where only the hodoscope horizontal strip # 3 is crossed by the beam.

Once we are sure that the beam crosses only one pad, the measurement of the crosstalk essentially consists in determining:

- in which fraction of events more than one pad is hit;
- if the multiple hit pads are adjacent one to each other (i.e. if they form a cluster);
- if the secondary hits are in-time respect to the primary one. We define in-time crosstalk the secondary signals delayed by $\Delta t < 20$ ns; if $\Delta t > 20$ ns, we speak of out-of-time crosstalk.

First, in Fig.17 (LEFT) we plot the average number of hit pads as function of the high voltage setting.

In Fig.17 (RIGHT) we show the fraction of events with multiple contiguous hits. The multiple hits are most of the times due to adjacent pads (see also Table 3). So, the average event multiplicity is a good measurement of the average cluster multiplicity (or cluster size).

Then, for cathode and wire pads, we compared the time spectra in events with exactly one hit with the spectra for multiple hits. Results are shown in Fig. 18. Once the geometrical selection with the hodoscope is imposed, the tails of the time spectra are entirely due to multiple hit events.

Finally, in events with two hit pads, we measured the time delay between the second signal and the first one. This allowed to calculate the fraction of crosstalk in-time ($\Delta t < 20$ ns) and out-of-time, respect to the total number of events selected only with the hodoscope. Results are shown in Fig. 19 for cathode pads. The in-time crosstalk is 8.1% at 3150 V.

The choice of the cathode pad threshold should minimise the crosstalk and at the same time guarantee a satisfactory value of the efficiency. From Fig.20 we see that 300 mV is a good working point for cathode pads. A lower value provides a slight improvement on the efficiency but a clearly worst crosstalk fraction.

For the study of the crosstalk between the wire pads, we followed the same procedure as for cathodes. In Fig. 21 we plot the time delay between the second signal and the first one, in events with two hit pads, for two different thresholds; a second peak is clearly visible at later time.

The fraction of crosstalk in-time and out-of-time, respect to the total number of events selected only with the hodoscope, is shown in Fig. 22 and is summarised in Table 4 for HV=3150 V. Results are compatible with those in reference [2].

We scanned the vertical Y axis in a range of about 15 cm, for high voltage HV=3150 V. This

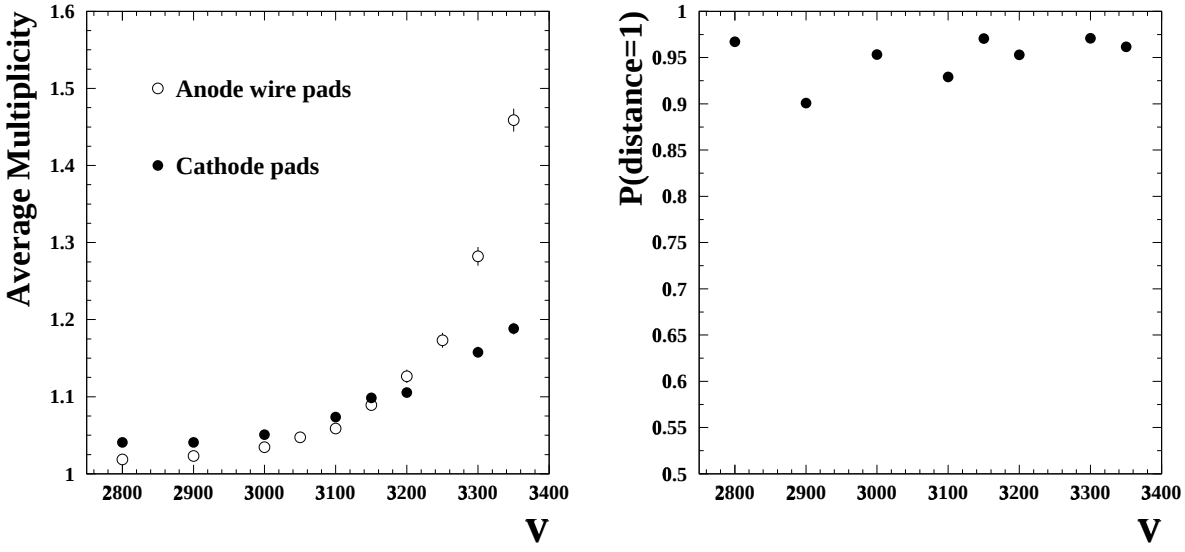

Figure 17: LEFT: Average number of hits, for cathode pads and wire pads, as function of the high voltage setting. RIGHT: Probability of hit in nearby pads in events with hit multiplicity > 1, for cathode pads. Thresholds are: Cathodes=300 mV Wires=350 mV.

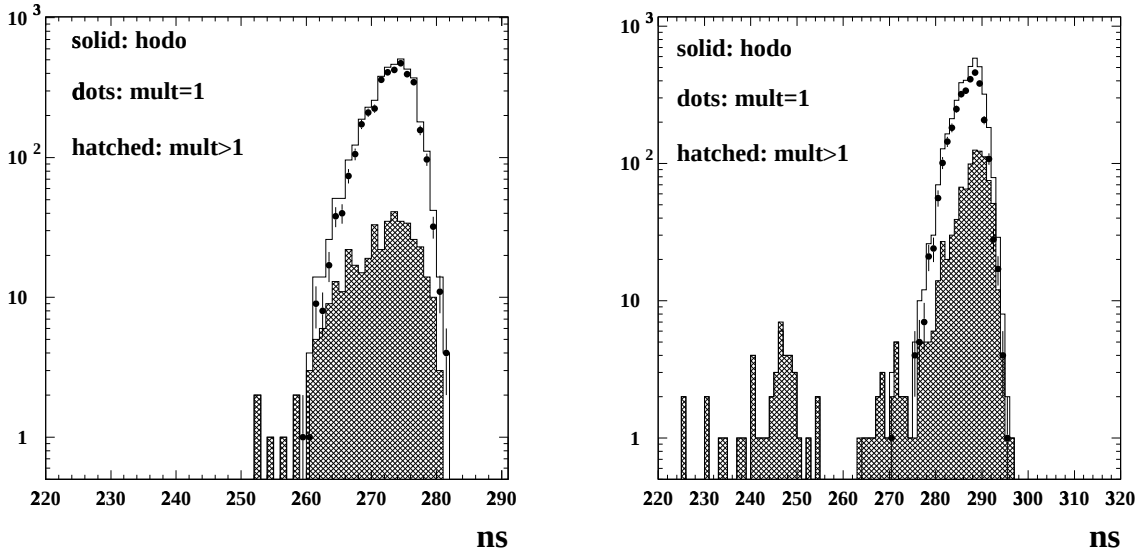

Figure 18: Time spectra for (left) single cathode pad and (right) single wire pad. Solid line: only geometrical selection with hodoscope. Dots: hodoscope selection and hit multiplicity = 1. Hatched: hodoscope selection and hit multiplicity > 1. High voltage is 3150 V; thresholds are: Wires=350 mV Cathodes=300 mV.

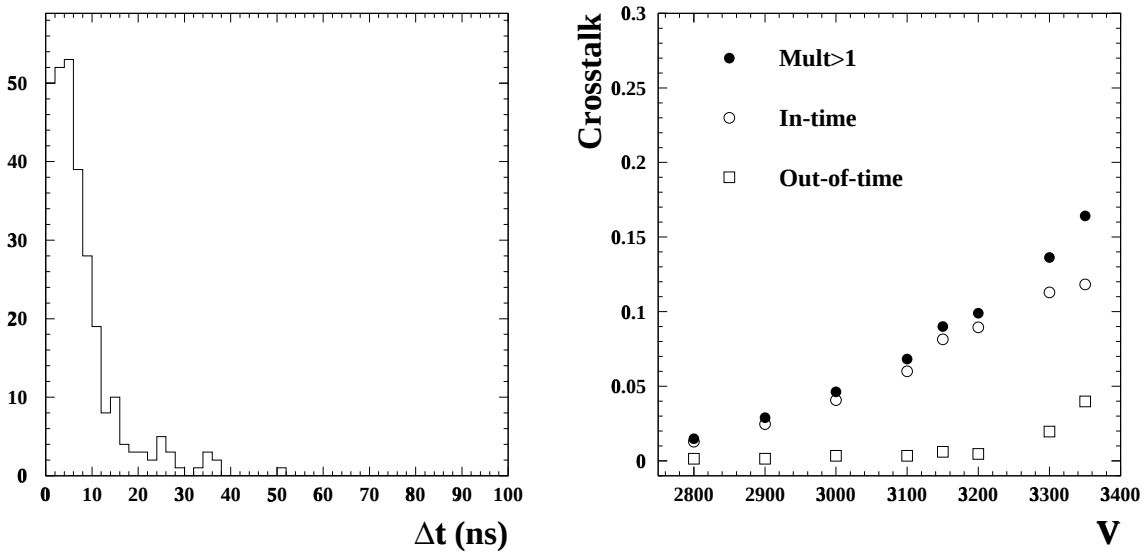

Figure 19: LEFT: Time delay between the second and the first hit in events with two hits, for cathode pads. RIGHT: crosstalk fraction as function fo the high voltage setting. (full dots) fraction of multiple hit events; (empty dots) fraction of in-time crosstalk; (squares) fraction of out-of-time crosstalk. Threshold is 300 mV.

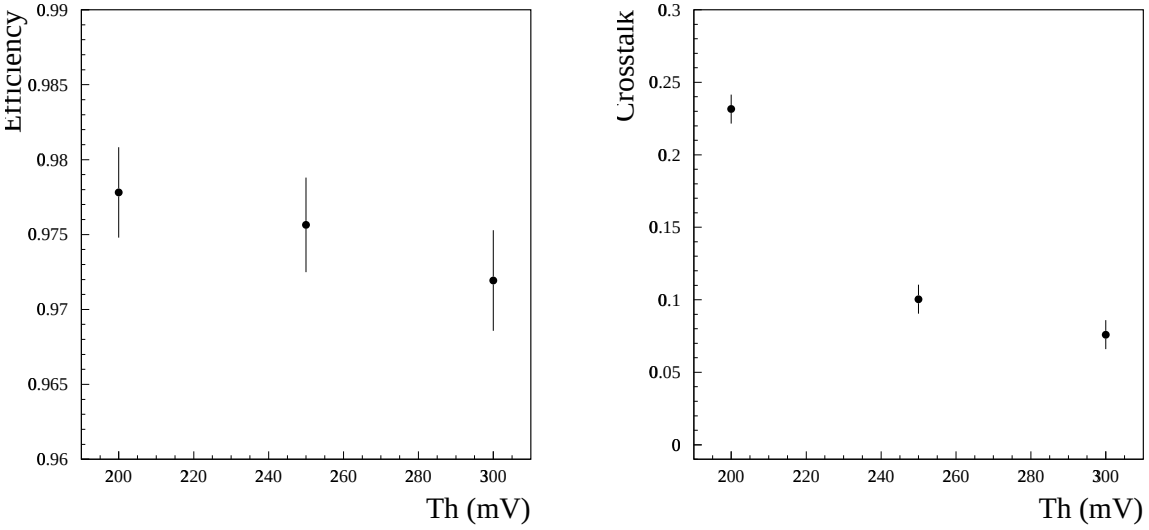

Figure 20: Efficiency (left) for the single cathode pad and (right) fractional in-time crosstalk, as function of the cathode pad threshold. High Voltage setting is fixed at 3150 V.

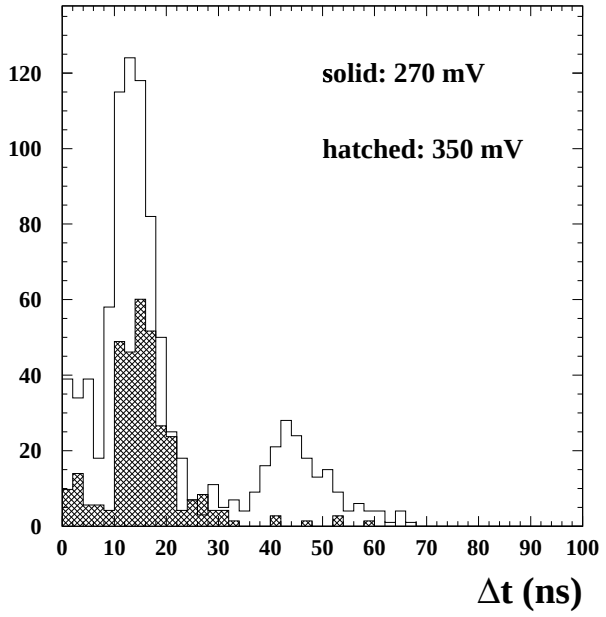

Figure 21: Time delay between the second and the first hit in events with two hits, for wire pads, for two different thresholds, at a fixed HV setting (3150 V).

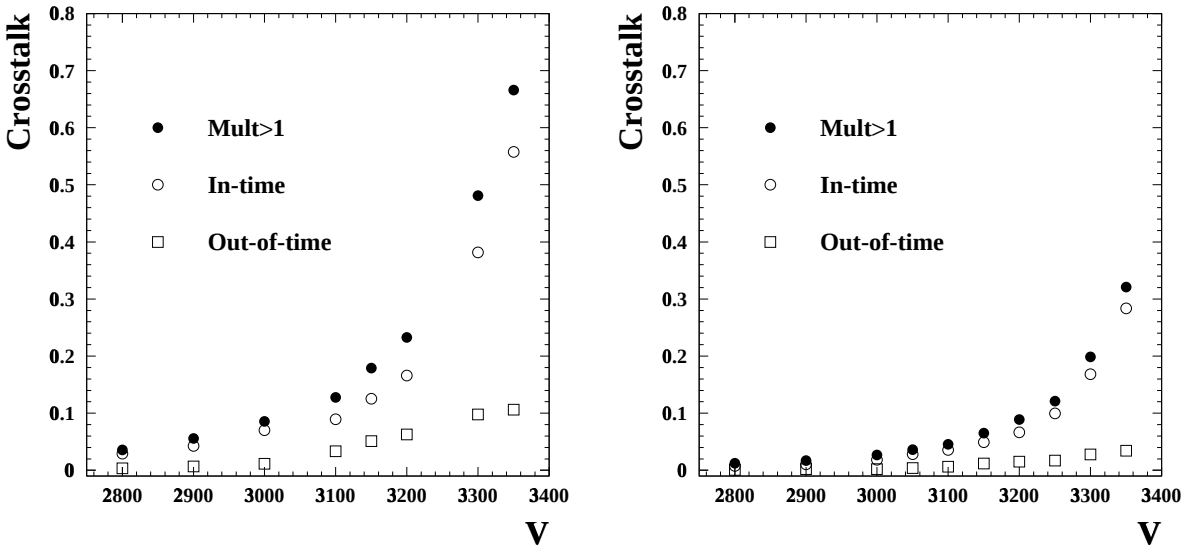

Figure 22: Crosstalk fraction as function of the high voltage setting, for wire pads. LEFT: threshold=270 mV; RIGHT: threshold=350 mV. (full dots) fraction of multiple hit events; (empty dots) fraction of in-time crosstalk; (squares) fraction of out-of-time crosstalk. High voltage is 3150 V.

High Voltage (V)	Wire pads	Cathode pads
3000	$92.1 \pm 1.8\%$	$95.0 \pm 1.6\%$
3200	$96.6 \pm 0.8\%$	$95.0 \pm 1.1\%$
3350	$98.9 \pm 0.4\%$	$96.0 \pm 0.8\%$

Table 3: Requiring that exactly two pads provide a signal, the table contains the fraction of events in which these pads are adjacent (for several high voltage settings). Thresholds are 270 mV (Wires) and 300 mV (Cathodes).

Threshold (mV)	350	270
In-time	4.9%	12.5%
Out-of-time	1.2%	5.1%

Table 4: Fraction of crosstalk in-time and out-of-time, for wire pads, at two different threshold settings, for high voltage HV=3150 V.

allowed to measure the fraction of crosstalk for different impinging point of the beam on the pad (at the center, near the edge, etc...).

Results are reported in Fig. 23. At the first chamber position of the Y scan (Y=0), selecting the hodoscope horizontal strip # 3, the beam is focused at the center of cathode pad # 7 and at the center of wire pad # 2. As expected, at Y=0 the crosstalk is at a minimum. The peaks in the plots correspond to pad edges, the minima to pad centers. The distance between the peaks is equal to pad width (2.5 cm). From the minima positions, the edge of last pad is expected to be at Y=-3.75.

The efficiency as function of the detector vertical position Y is shown in Fig.24. The efficiency increases from 0 to 1 in a Y range of $\sim$ 2 cm. The observed shape is due to the convolution of the beam width (around 1 cm, almost flat), with some edge effect due to the chamber. More investigation is needed in order to disentangle the two contributions, possibly using a narrower beam selection.

3.7 Study of the spatial uniformity

We performed a preliminary measurement of the chamber uniformity, moving the detector in the plane perpendicular to the beam direction.

To understand if the detector response is the same for any beam position along the pad direction, we moved the chamber along the horizontal X axis in a range of about 26 cm. We selected a limited X spread of the beam requiring a single hodoscope vertical strip fired. The high voltage was set at 2800 V, below the plateau, to have a higher sensitivity of efficiency on gain changes. Results of the scan are shown in Fig.25. Concerning cathode pads is clearly visible the fact that only one half of the detector is readout.

For wire pads, where we explore the whole detector plane, we observe a spread of the efficiency in the range 55-70% (edge effect excluded), which in Fig. 12 corresponds to ± 25V uncertainty around the 2800 V working point. The same uncertainty produces a negligible effect on the efficiency if a working point on the plateau is chosen (see Fig. 11).

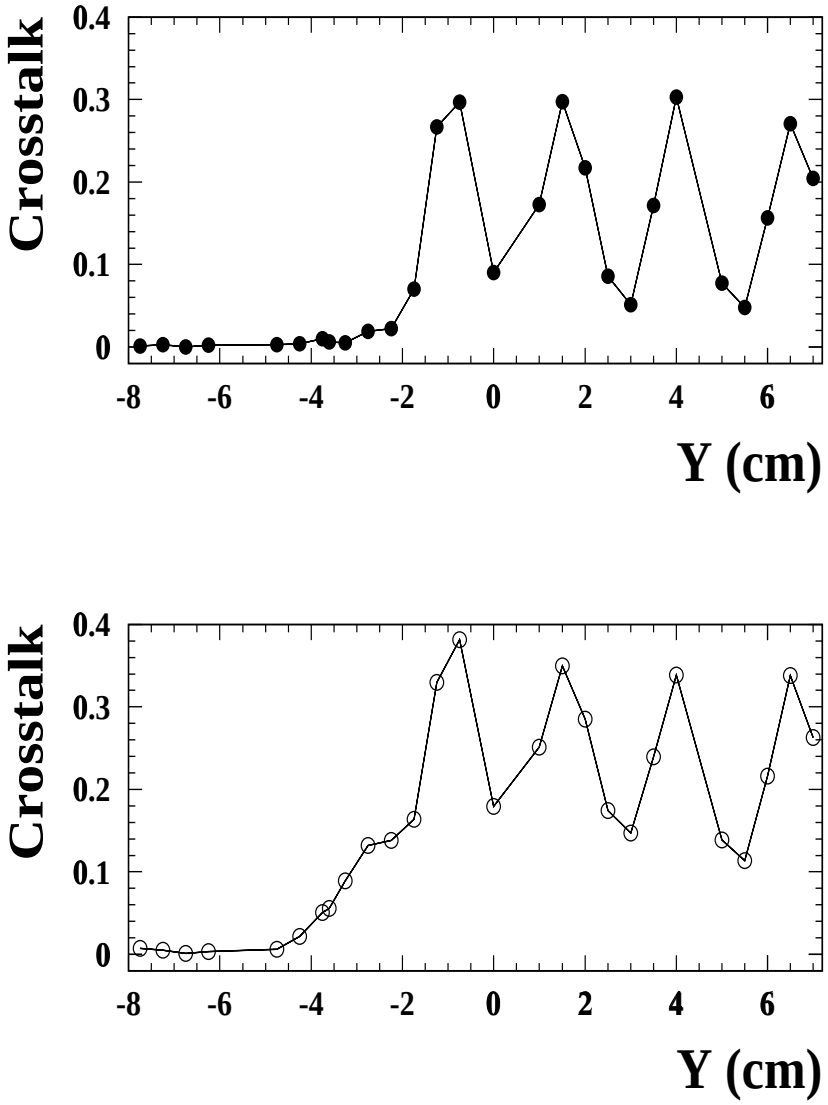

Figure 23: Crosstalk for (full dots) cathode pads and (empty dots) wire pads, as function of the detector vertical position Y. The peaks in the plots correspond to pad edges, the minima to pad centers. The distance between the peaks is equal to pad width (2.5 cm). Edge of last pad is at Y=-3.75. High Voltage is 3150 V. Thresholds are: Cathodes=300 mV Wires=270 mV.

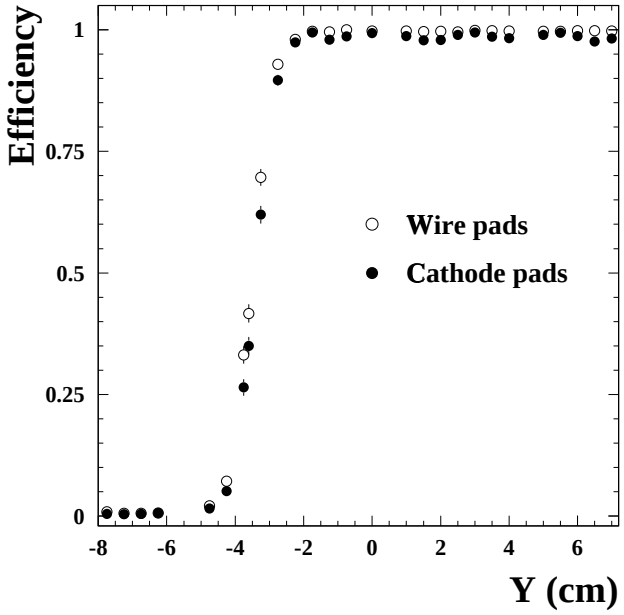

Figure 24: Efficiency for (full dots) cathode pads and (empty dots) wire pads, as function of the detector vertical position Y. Edge of last pad is at Y=-3.75. High Voltage is 3150 V. Thresholds are: Cathodes=300 mV Wires=270 mV.

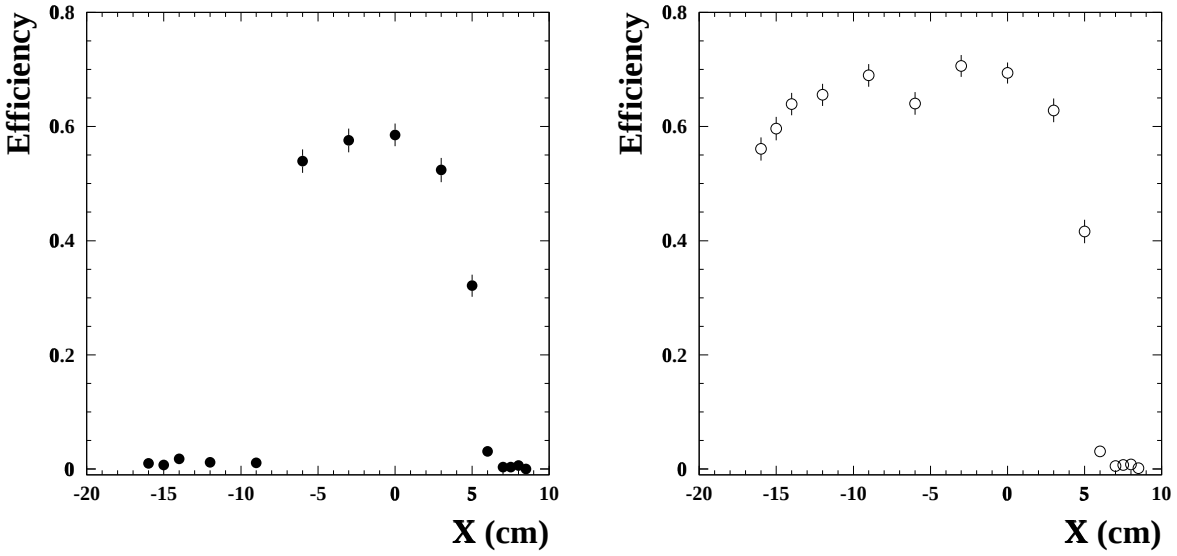

Figure 25: Efficiency for (left) cathode pads and (right) wire pads, as function of the detector horizontal position X. Hodoscope pads selected are: vertical=5; horizontal=3 and 4. High Voltage is 2800 V. Thresholds are: Cathodes=250 mV Wires=350 mV.

4 Conclusions

The results obtained in this testbeam are very satisfactory, and comparable with the one obtained with other prototypes [3, 2].

The prototype performances - high efficiency, low current, good time resolution, low crosstalk effect - are encouraging.

They confirm the validity of the mechanical design and of the construction procedures and represent a good starting point for the construction of a bigger prototype for the regions R3 and R4.

Acknowledgements

We thank Anatoli Kashchuk for providing ASDQ++ boards and help in making them operational, and Werner Riegler, Burkhard Schmidt and Thomas Schneider for their help in the setup of the test.

Appendix: results from the testbeam of a quadrigap

Experimental setup

At the end of September 2001, a prototype quadrigap was brought to CERN. It was composed of two bigaps: the first (AB) was the bigap tested in July (and described above in this note), the second was a new bigap (CD). Only the Cathode Pads were read out. We found that the bigap AB was not working properly: it was noisy and not fully efficient, due to bad cabling of FEE. On the other hand, the bigap CD showed a very good behaviour (efficiency, time resolution, etc...), working at a lower threshold respect to July testbeam: only 180 mV for Cathode Pads, compared to 300 mV in July.

In this appendix, we want to briefly report the measurements for bigap CD and to compare them with the results of AB. However, as we will show below, most of the measurements are dependent on the vertical position Y at which the particle crosses the chamber, except for efficiency (for which this dependence is weak). For this reason, a comparison between AB and CD bigaps is possible only at the same Y value.

We must mention that in September testbeam (i.e. for CD) a scintillator horizontal finger (of width $\sim 0.5cm$) was available for a precise selection of the beam vertical coordinate. Instead, in the July testbeam (i.e. for AB), the finger was not available: the results shown refer to events selected only with the hodoscope (requiring only horizontal strip # 3), and thus with a worst precision ($\sim 1cm$).

Efficiency

In Fig. 26 the efficiencies of the bigaps are shown as function of the vertical coordinate Y. For CD, we scanned the Y axis in a range of about 5 cm, corresponding to the width of two pads. The high voltage was HV=3.15 kV. As expected, the efficiency slightly decreases in correspondence of the pad edges. The average efficiency, integrating over the two contiguous pads 1 and 2 is ~ 0.987 for AB and ~ 0.994 for CD.

In Fig. 27 we show the efficiency plateaux. We compare AB and CD even though the particle position respect to the chamber cannot be identical. As expected the bigap CD, working at lower threshold (180 mV), is more efficient than AB. For HV $>$ 3.1 kV, the efficiency is $\epsilon > 99\%$.

The efficiency plateaux for each gap (A,B,C,D) are shown in Fig. 28. Here the A and B gaps were operating at threshold 250 mV. With threshold 180 mV, the efficiency is $\epsilon > 95\%$ for HV $>$ 3.2 kV. The various gaps have similar response, showing a very good uniformity.

The dependence of the efficiency on the cathode pad threshold for the bigap CD is shown in Fig. 29 at a fixed high voltage (3.15 kV) and for two different methods: 'Single Pad' (only the pad with more hits is considered) and 'First Hit' (only the first hit in time is considered). For 180 mV threshold, $\epsilon \sim 0.997$.

Crosstalk and cluster size

We also measured the crosstalk, that we defined as the fraction of events with two adjacent pads hit within a time window of 20 ns (in-time hits). The crosstalk is the sum of two effects: a geometrical one (depending on the particle vertical position Y) and an intrinsic one (due to electrical coupling between the pads). For this reason, a comparison between AB and CD bigaps is possible only at the same Y value.

In Fig. 30 we compare the crosstalk in bigaps AB and CD, as function of the particle vertical position Y. As a consequence of finger selection, the Y dependence of crosstalk is steeper for

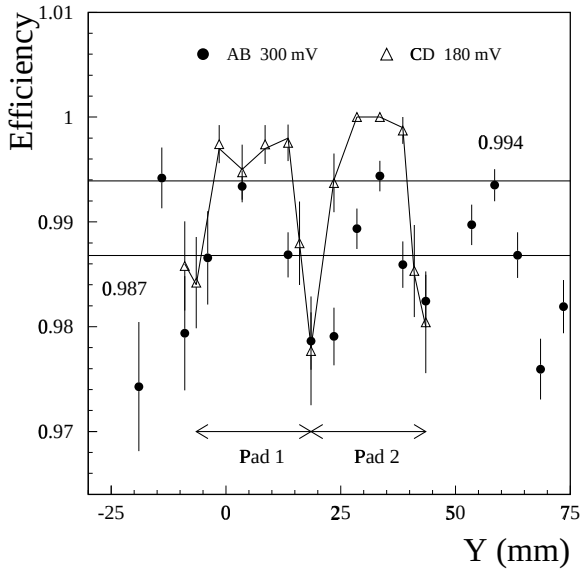

Figure 26: Cathode Pad efficiency, as function of the particle vertical position Y, for bigaps AB and CD, determined with the first hit in time. As expected, the efficiency slightly decreases in correspondence of the pad edges. The average efficiency, integrating over the two contiguous pads 1 and 2 is ~ 0.987 for AB and ~ 0.994 for CD.

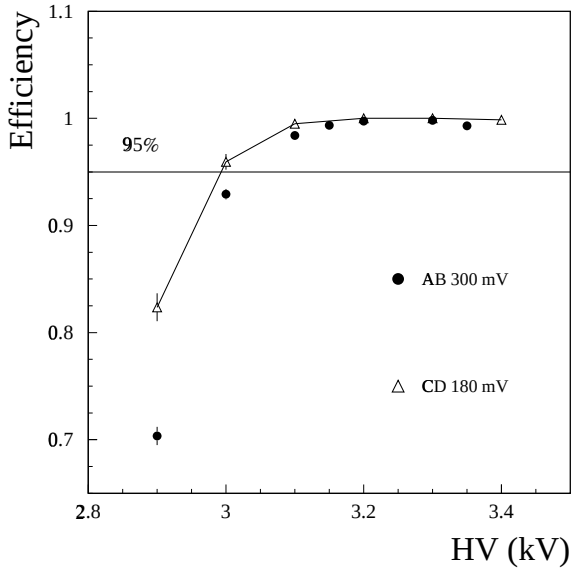

Figure 27: Cathode Pad efficiency, as function of the high voltage setting, for bigaps AB and CD, determined with the first hit in time. The lines connecting together the CD values, are drawn to guide the eye.

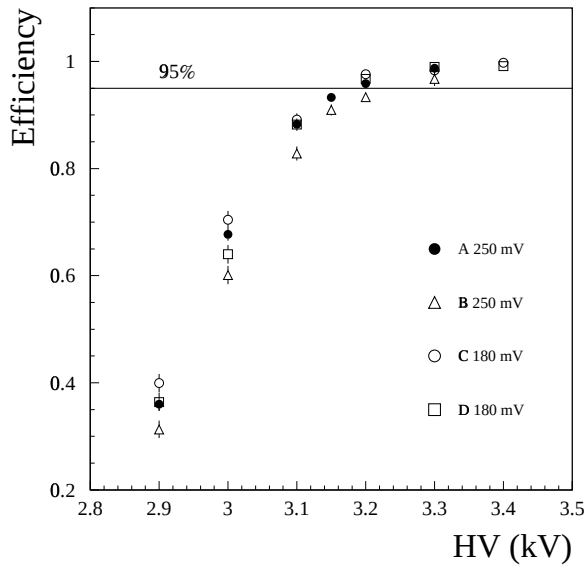

Figure 28: Cathode Pad efficiency, as function of the high voltage setting, for each gap A,B,C and D, determined with the first hit in time.

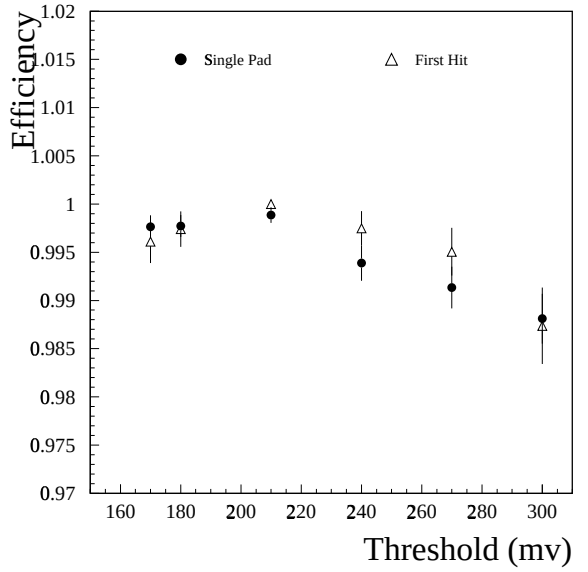

Figure 29: Cathode Pad efficiency of bigap CD, as function of the circuit threshold setting, at a fixed high voltage (3.15 kV) and for two different methods: 'Single Pad' (only the pad with more hits is considered) and 'First Hit' (only the first hit in time is considered).

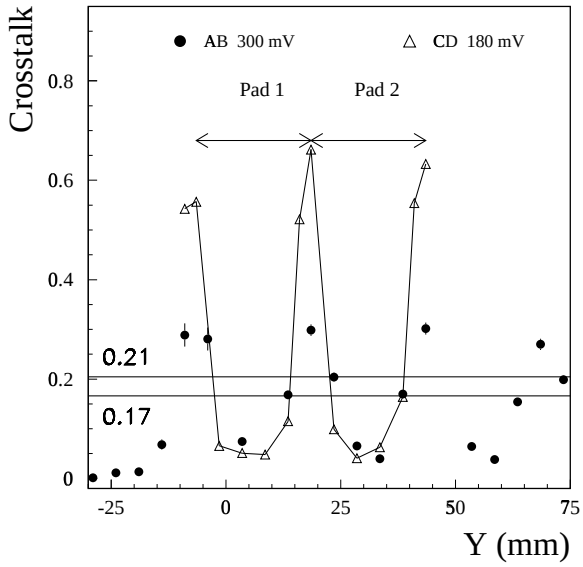

Figure 30: In-time crosstalk in bigaps AB and CD, as function of the particle vertical position Y, at a fixed high voltage (3.15 kV). The peaks correspond to pad egdes. The average crosstalk, integrating over the two contiguous pads 1 and 2 is ~ 0.17 for AB and ~ 0.21 for CD. Statistical errors are negligible.

CD (the peaks correspond to pad egdes). The higher value of crosstalk in CD is essentially due to the lower circuit threshold. The average crosstalk, integrating over the two contiguous pads 1 and 2 is ~ 0.17 for AB and ~ 0.21 for CD.

The next figure (Fig. 31) is a detailed zoom over this plot, showing the gap between the two pads (where the crosstalk is maximum) for bigap CD. Here Y=0 at the Pad 2 lower edge. The data are compared to a calculation based on the distribution of the collected charge as function of the incident particle position respect to the pad edge (see Fig.5.1 in [4]). We assumed that the pad efficiency increases linearly from 0 to 1 when the fraction of charge collected increases from 0 to 20%. Even using such a rough model, the agreement between measurement and calculation is good.

In Fig. 32 we show the distribution of the number of in-time hits for two incident particle vertical positions: at the center of a pad (condition of minimum crosstalk) and at the edge of a pad (maximum crosstalk). The difference in the particle positions reflects mainly in the ratio between double and single hit events. In both cases the fraction of events with more than 2 hits is $< 5\%$.

Moreover, when two hits are present, they are almost always in adjacent pads. For this reason, the hit multiplicity is often called 'Cluster Size'. The average cluster size shows a behaviour qualitatively similar to crosstalk, as illustrated in Fig. 33. The average cluster sizes, obtained integrating over the two contiguous pads 1 and 2 are 1.15 in AB and 1.26 in CD.

The dependence of cluster size on the high voltage applied is shown in Fig. 34, for the CD bigap and for each single gap C and D, at a fixed particle position. The behaviours of the two gaps are very similar.

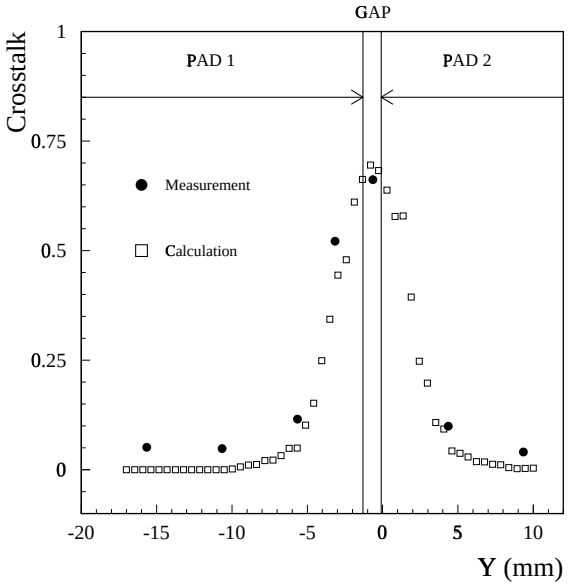

Figure 31: Crosstalk in bigap CD, as function of the particle vertical position Y (Y=0 at the Pad 2 lower edge). High voltage is 3.15 kV and threshold is 180 mV. The measurements are compared to a calculation based on the fractional charge collected by the two pads (see text). Statistical errors are negligible.

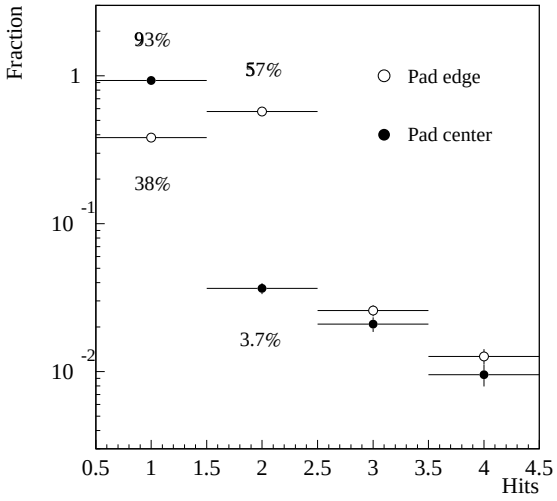

Figure 32: Probability distribution of the number of in-time hits for two incident particle vertical positions: at the center of a pad and at the edge of a pad. The difference in the particle positions reflects mainly in the ratio between double and single hit events. Measurements are for bigap CD, at fixed high voltage (3.15 kV) and threshold (180 mV).

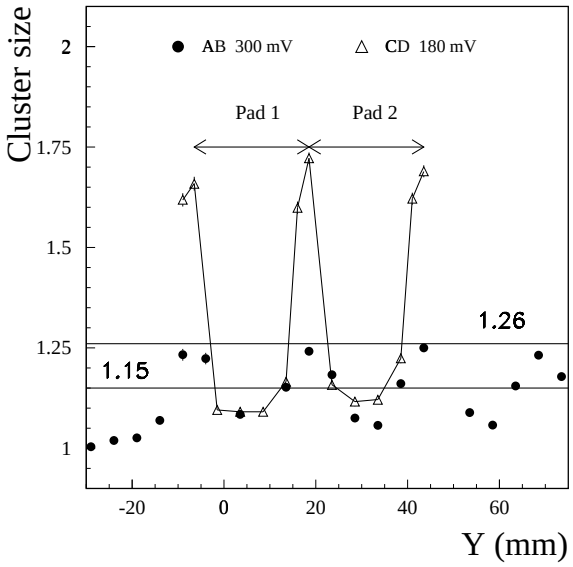

Figure 33: Average cluster size in bigaps AB and CD, as function of the particle vertical position Y, at a fixed high voltage (3.15 kV). Only in-time hits were considered (i.e. hits in a 20 ns time window). The average over the two contiguous pads 1 and 2 is 1.15 for AB and 1.26 for CD.

In Fig. 35 we show the average cluster size as function of the circuit threshold, for bigap CD, for a particle crossing approximately the center of a pad. In this condition, the minimum crosstalk and cluster size are expected.

Time resolution

We measured also the time resolution, assuming that it is well represented by the root mean square of the time spectrum (the 'Single Pad' spectrum, i.e. only the pad with more hits is considered). The comparison between AB and CD is shown in Fig. 36. As for crosstalk, the higher threshold of AB implies a smoother dependence on the position. As expected, the time resolution is larger when the particle crosses a pad close to the edge. The average over the two contiguous pads 1 and 2 is ~ 4.24 ns for AB and ~ 3.49 ns for CD.

The time resolution is also sensitive on high voltage. This is shown in Fig. 37, for the CD bigap and for each single gap C and D, at a fixed particle position. The behaviours of the two gaps are very similar.

We also measured the effect on the time resolution of changing the circuit threshold. The results are shown in Fig. 38 for a fixed particle position and high voltage. The rms increases almost linearly from $\sim 2.95ns$ at 170 mV, to $\sim 3.67ns$ at 300 mV.

Chamber uniformity

After the testbeam, we brought back the quadrigap chamber to Frascati labs and recovered the AB operation. We measured the current in each gap A,B,C,D moving a radiation source in different positions on the top gap cover panel. Two setups were considered: ABCD (with A on top and the source moved over its cover) and DCBA (with D on top).

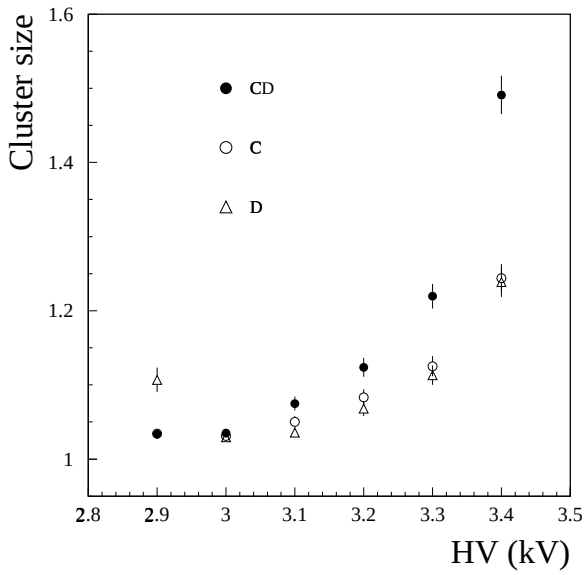

Figure 34: Average cluster size of in-time hits in CD and in each single gap C and D, as function of high voltage, at a fixed particle position Y. The threshold is 180 mV.

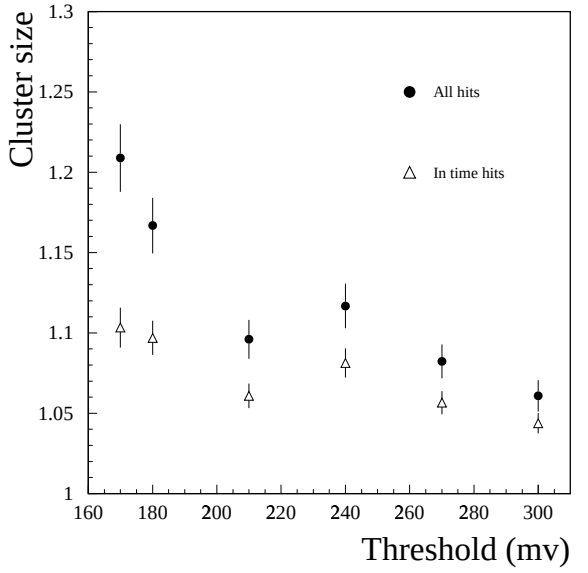

Figure 35: Average cluster size as function of the circuit threshold, for bigap CD, for a particle crossing approximately the center of a pad, at fixed high voltage 3.15 kV. Only in-time hits were considered.

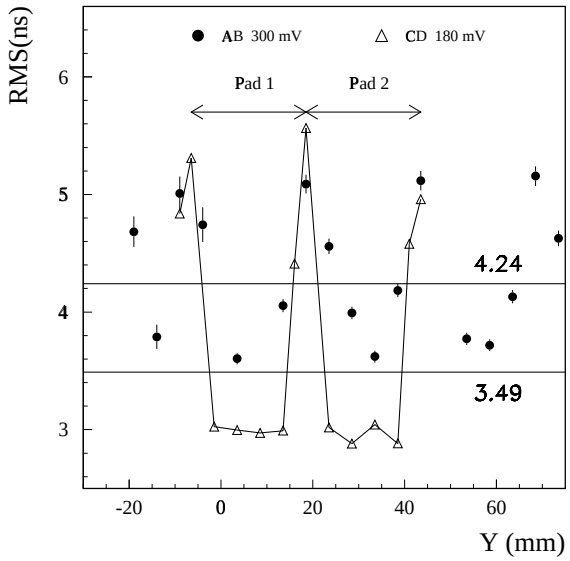

Figure 36: Time resolution of AB and CD bigaps as function of the particle vertical position, at fixed high voltage (3.15 kV) and thresholds. RMS is defined as the root mean square of the 'Single Pad' time spectrum (i.e. only the pad with more hits is considered). The average over the two contiguous pads 1 and 2 is ~ 4.24 ns for AB and ~ 3.49 ns for CD. Statistical errors for CD are not shown.

Two different sources were used: a non collimated Co60 source of ~ 19 MBq and a collimated Sr90 source of ~ 0.94 MBq. Two set of measurements were done: the source was moved over the top cover of the quadrigap, with A on top and D at the bottom and viceversa. With the first source we measured the current in each gap A,B,C,D for 9 different positions (numbered 0,1,...,8) of the source over the top cover of the quadrigap, as shown in Fig. 39 (for A on top). In Fig. 40 we show the current in gap A, as function of the high voltage, for Co60 source on top of the gap, in the central position 0. The dependence of currents on the position is shown in Fig. 41 for each gap, normalized to the average currents: $i_A = 35\ nA$, $i_B = 31.5\ nA$, $i_C = 30.8\ nA$, $i_D = 34\ nA$.

The collimated Sr90 source was placed in 17 different positions (the center of each pad 1,2,...,16 and the center of the plane, indicated with 0), as shown in Fig. 39 (for A on top). The dependence of currents on the position is shown in Fig. 42 for each gap, normalized to the average currents: $i_A = 8.1\ nA$, $i_B = 5.8\ nA$, $i_C = 5.9\ nA$, $i_D = 8.6\ nA$.

These measurements show that, at least for this chamber dimension, the construction technology allows to stay largely inside the 20% uniformity requirements of the LHCb Muon TDR.

References

[1] Muon TDR, CERN/LHCC 2001-010, 28 May 2001.
[2] LHCb-MUON 2001-024, 15 May 2001.
[3] LHCb-MUON 2000-003, 14 February 2000.
[4] LHCb-MUON 2000-061, 8 October 2000.

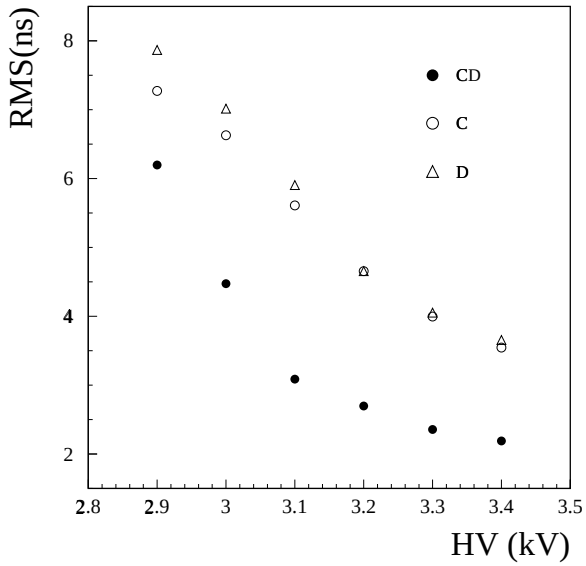

Figure 37: Time resolution as function of the high voltage, for the CD bigap and for each single gap C and D. Chamber vertical position and circuit threshold (180 mV) are fixed. RMS is defined as the root mean square of the time spectrum (the 'Single Pad' spectrum, i.e. only the pad with more hits is considered). Statistical errors are not shown.

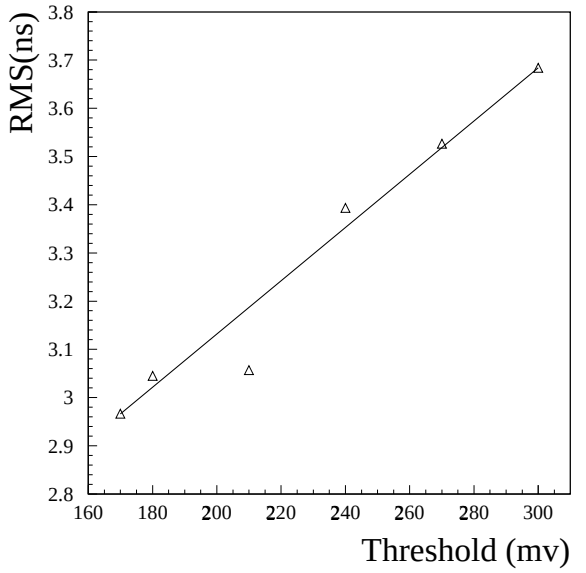

Figure 38: Single pad time resolution for bigap CD, as function of the circuit threshold. Chamber vertical position and high voltage (3.15 kV) are fixed. The line is drawn to guide the eye. The rms increases almost linearly from $\sim 2.95ns$ at 170 mV, to $\sim 3.67ns$ at 300 mV. Statistical errors are not shown.

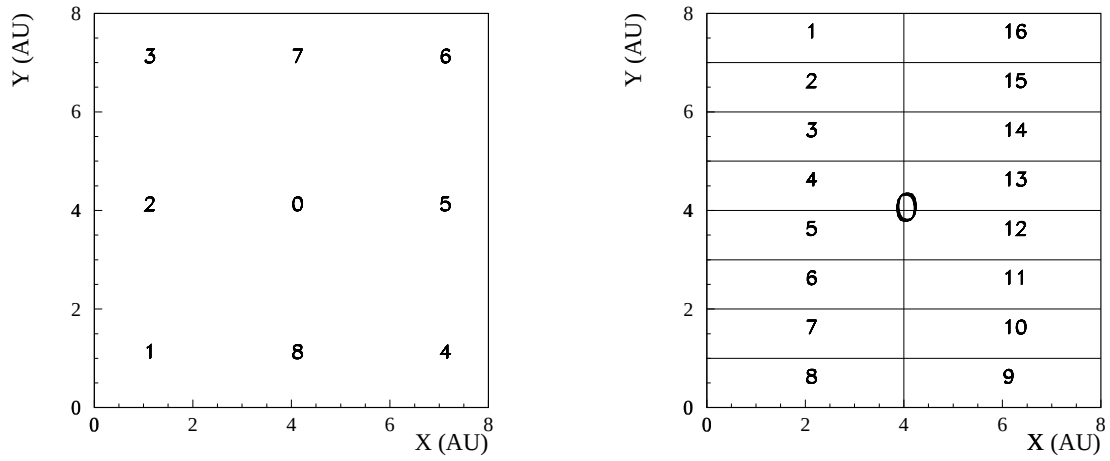

Figure 39: Positions of the sources moved over the top cover of the ABCD quadrigap (A on top). LEFT: positions 0,1,2,..,8 of the Co60 source. RIGHT: positions of the Sr90 source at the center of the plane (0) and in correspondence of each pad (1,2,...,16).

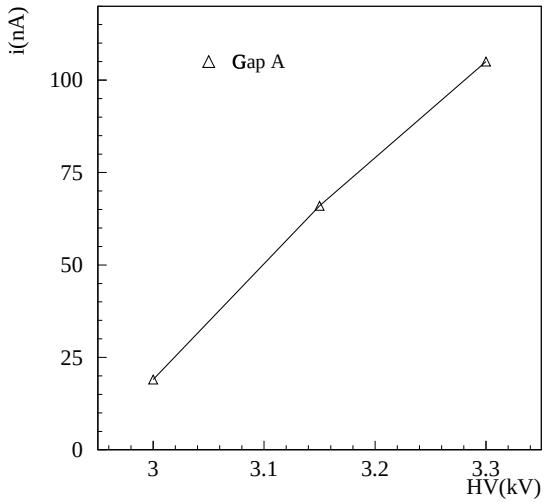

Figure 40: Dependence of current in the gap A on the high voltage, for the Co60 source in central position (on the cover of A gap). Line is drawn to guide the eye.

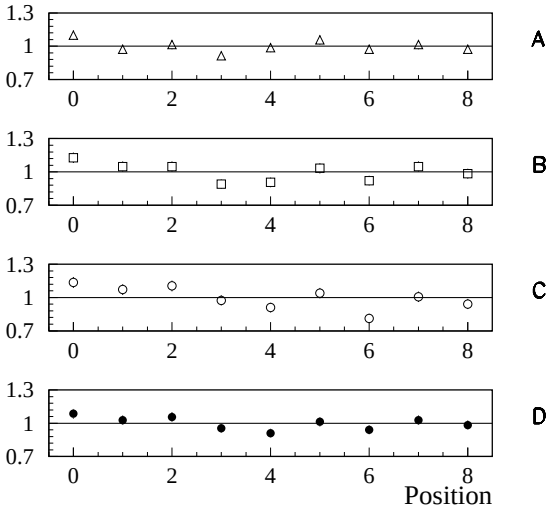

Figure 41: Dependence of currents in each gap on the position of the Co60 source, normalized to the average currents: $i_A = 35\ nA$, $i_B = 31.5\ nA$, $i_C = 30.8\ nA$, $i_D = 34\ nA$, with the source on top of A and on top of D.

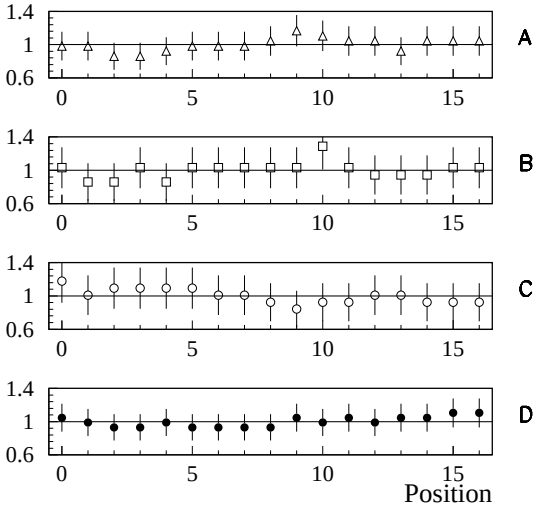

Figure 42: Dependence of currents in each gap on the position of the Sr90 source, normalized to the average currents: $i_A = 8.1\ nA$, $i_B = 5.8\ nA$, $i_C = 5.9\ nA$, $i_D = 8.6\ nA$, with the source on top of A and on top of D.